energies

MDPI

Article

Modular Rotor Single Phase Field Excited Flux Switching Machine with Non-Overlapped Windings

Lutf Ur Rahman [1,*], Faisal Khan [1], Muhammad Afzal Khan [1], Naseer Ahmad [1], Hamid Ali Khan [1], Mohsin Shahzad [1], Siddique Ali [2] and Hazrat Ali [1]

[1] Department of Electrical and Computer Engineering, COMSATS University Islamabad, Abbottabad Campus, University Road Abbottabad, Abbottabad 22060, Pakistan; faisalkhan@cuiatd.edu.pk (F.K.); afzalk0370@gmail.com (M.A.K.); n.ahmadmwt@gmail.com (N.A.); hamidalims@gmail.com (H.A.K.); mohsinshahzad@cuiatd.edu.pk (M.S.); hazratali@cuiatd.edu.pk (H.A.)

[2] Department of Electrical Engineering, University of Engineering and Technology Peshawar, Peshawar 25120, Pakistan; siddique.ali@uetpeshawar.edu.pk

* Correspondence: lutfurrahman65@yahoo.com

Received: 15 December 2018; Accepted: 11 April 2019; Published: 25 April 2019

Abstract: This paper aims to propose and compare three new structures of single-phase field excited flux switching machine for pedestal fan application. Conventional six-slot/three-pole salient rotor design has better performance in terms of torque, whilst also having a higher back-EMF and unbalanced electromagnetic forces. Due to the alignment position of the rotor pole with stator teeth, the salient rotor design could not generate torque (called dead zone torque). A new structure having sub-part rotor design has the capability to eliminate dead zone torque. Both the conventional eight-slot/four-pole sub-part rotor design and six-slot/three-pole salient rotor design have an overlapped winding arrangement between armature coil and field excitation coil that depicts high copper losses as well as results in increased size of motor. Additionally, a field excited flux switching machine with a salient structure of the rotor has high flux strength in the stator-core that has considerable impact on high iron losses. Therefore, a novel topology in terms of modular rotor of single-phase field excited flux switching machine with eight-slot/six-pole configuration is proposed, which enable non-overlap arrangement between armature coil and FEC winding that facilitates reduction in the copper losses. The proposed modular rotor design acquires reduced iron losses as well as reduced active rotor mass comparatively to conventional rotor design. It is very persuasive to analyze the range of speed for these rotors to avoid cracks and deformation, the maximum tensile strength (can be measured with principal stress in research) of the rotor analysis is conducted using JMAG. A deterministic optimization technique is implemented to enhance the electromagnetic performance of eight-slot/six-pole modular rotor design. The electromagnetic performance of the conventional sub-part rotor design, doubly salient rotor design, and proposed novel-modular rotor design is analyzed by 3D-finite element analysis (3D-FEA), including flux linkage, flux distribution, flux strength, back-EMF, cogging torque, torque characteristics, iron losses, and efficiency.

Keywords: flux switching machine; modular rotor; non-overlap winding; magnetic flux analysis; iron losses; copper loss; stress analysis; finite element method

1. Introduction

In everyday applications, universal motors are mostly used in such devices as power tools, blenders, and fans. They are operated at high speed and deliver high starting torque as getting direct power from the ac-grid. At high speeds, universal motors cause noise due to their mechanical commutators, and they have a comparatively short maintenance period. To cope with these snags, research of a high-performance and low-cost brushless machine is greatly in demand [1,2]

Switched-flux brushless machines, a new class of electric machine were first presented in the 1950s [3]. Flux switching machines (FSMs), an unconventional machine, originated from the combination of principles among induction alternator and switched reluctance motor [4]. Distinct features of FSMs are their high torque density and robust rotor structure resulting from putting all excitation on the stator. In the past decade, various novel FSMs have been developed for several applications, confines from domestic appliances [5], automotive application [6,7], electric vehicles [8,9], wind power, and aerospace [10]. FSMs are categorized into permanent magnet flux switching machines (PMFSM), field excited flux switching machines (FEFSM), and hybrid excited flux switching machines (HEFSM). Permanent magnet FSMs and field excited FSMs have a permanent magnet (PM) and field excitation coil (FEC) for generation of flux source respectively, whilst both PM and FEC are generation sources of flux in HEFSM. The major advantage of FSMs is their simple/robust structure of rotor and easy management of temperature rise as all the excitation housed on stator. Recently, use of a permanent magnet as a primary source of excitation has dominated in flux switching research, due to their high torque/ high power density and optimum efficiency [11]. However, the maximum working temperature of PM is limited due to potential irreversible demagnetization. The use of PM in not always desirable due to high cost of rare earth material. For low cost applications, it is desirable to reduce the use of permanent magnets and hence they are replaced by DC-FEC. FEFSMs are capable of strengthening and weakening the generated flux as it is controlled by dc-current. FEFSMs have the disadvantage of less starting torque, fixed rotational direction, and high copper losses. The cumulative advantages of both FEC and PM are embedded in HEFSM having high torque capability/high torque density, HEFSMs also have high efficiency and flux weakening capability. However, the demerits of HEFSMs include a more complex structure, saturation of stator-core due to use of PM on stator, greater axial length, and high cost due to use of rare earth material. Therefore, FEFSMs could be considered a better alternative for requirements of low cost, wide speed controllability, high torque density, simple construction, less need of permanent magnet, and flux weakening operations as compared to other FSMs [12].

Numerous single-phase novel FS machines topologies has been developed for household appliances and different electric means. Single phase FSMs were first presented in [13] and further investigated in [14,15] by C. Pollock, they analyzed an 8S-4P doubly salient machine that offers high power density and low cost as shown in Figure 1. The FEC and armature has an overlapped winding arrangement resulting in longer end winding. To overcome the drawback of long end winding, the 12S-6P FSM has been developed that has same coil pitch as eight stator slots and four rotor poles but shorter end winding [16]. Figure 2 depicts how a 12-slot/6-pole machine has fully pitched winding arrangement as with C. Pollock's design. The end windings effect is even shorter by re-arranging the armature winding and FEC to different pitch of one and three slot pitches as shown in Figure 3. Both machines with F2-A2-six-pole and F1-A3-six-pole coil pitches have better copper consumption than a conventional machine (F2-A2-four-pole) for short axial length but has a disadvantage of higher iron loss due to more rotor poles [17]. The stator slots and rotor poles could be halved into F1-A3-3P machine as shown in Figure 4, that is more appropriate for high speeds due to a significant reduction in iron loss [16]. When the axial length is short, that is up to 25 mm, the average torque of both F2-A2/4P and six-pole machine is similar. However, F1-A3/3P exhibit higher average torque than F1-A3/6P machine at longer axial length of 60 mm. At the point when end winding is disregarded, a machine with fewer stator teeth and rotor poles has less average torque as compared to a machine with fewer rotor poles and stator slots for the same type of machine.

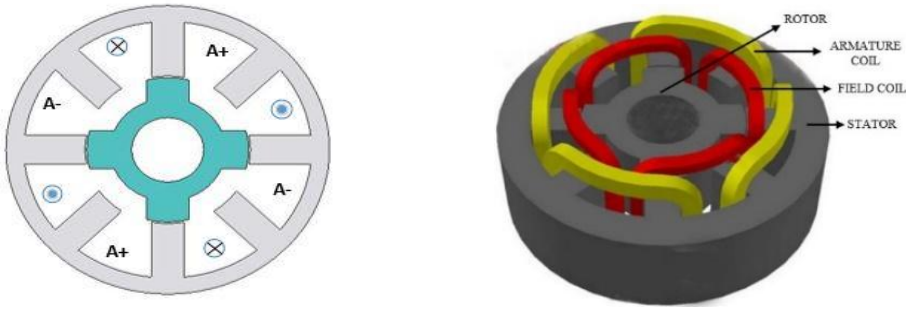

(**a**) (**b**)

Figure 1. 8S/4P FEFS machine (F2-A2-4P). (**a**) Cross-sectional model; (**b**) 3D model [16].

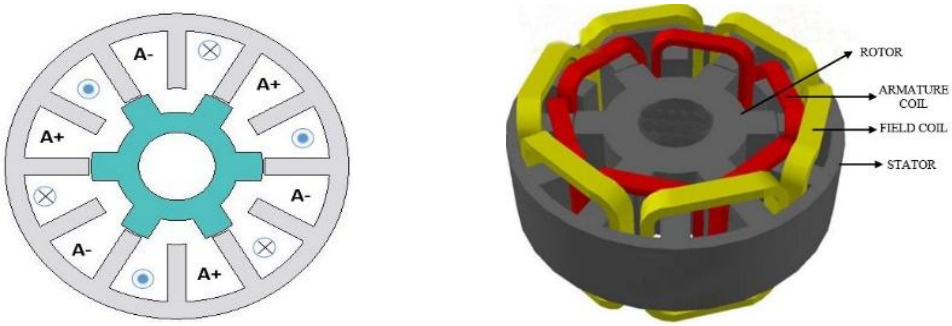

(**a**) (**b**)

Figure 2. 12S/6P FEFS machine (F2-A2-6P). (**a**) Cross-sectional model; (**b**) 3D model [16].

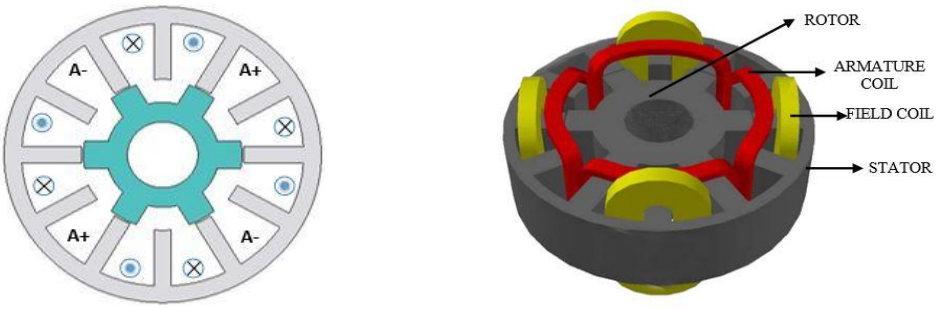

(**a**) (**b**)

Figure 3. 12S/6P FEFS machine with rearranged winding (F1-A3-6P). (**a**) Cross-sectional model; (**b**) 3D model [16].

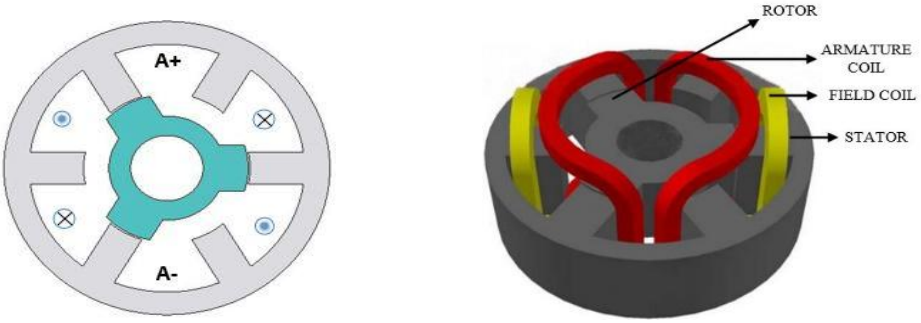

(**a**) (**b**)

Figure 4. 6S/3P FEFS machine (F1-A3-3P). (**a**) Cross-sectional model; (**b**) 3D model [16].

In single phase FS machines, torque is generated with doubly salient structure due to the tendency of rotor to align itself into a minimum reluctance position as shown in Figure 5. When the stator slot and rotor pole are aligned at a minimum reluctance position, the motor cannot generate torque (called 'dead zone of torque') at aligned positions unless armature current direction is reversed. The dead zone of torque is eliminated in [18] with sub-part rotor structure having different pole arc lengths. The eight-slot/four-pole sub-part rotors are merged on the same face and pole axes are not parallel. However, sub-rotor poles cannot be allied with stator slots at a same-time, thus reluctance torque is generated at any rotor position. The single phase 8S/4P sub-part rotor FSM only applicable for a situation that requires a continuous unidirectional rotation. The conventional sub-part rotor design has demerit of overlapped winding arrangements between FEC and armature winding that results in higher copper consumption and higher iron losses due to salient rotor structure. A single phase sub-rotor FS machine minimizes the advantage of high speed, as it cannot operate at speed higher than normal level.

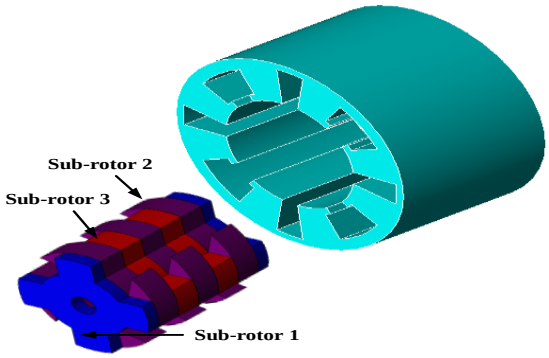

(**a**)

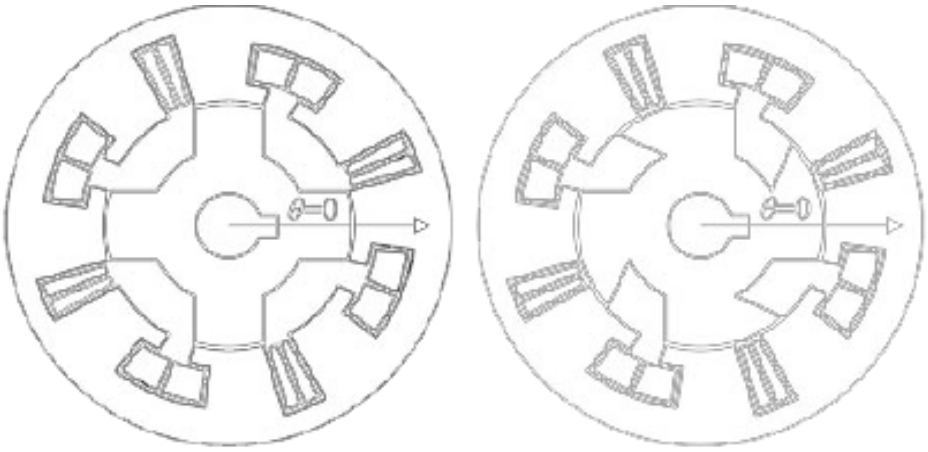

(**b**) (**c**)

Figure 5. Sub-part rotor structure. (**a**) Manifestation of sub-part rotor; (**b**) pole arc of sub rotor-1; (**c**) pole arc of sub rotor-2.

This paper presents a novel-modular rotor structure for single phase FS machines as shown in Figure 6. The proposed design comprises of non-overlapped winding arrangements between armature winding and FEC, and modular rotor structure. The consumption of copper is much reduced due to non-overlapped winding arrangements. The modular rotor single phase FSM exhibit a significant reduction in iron losses, also reduces the rotor mass and lower the use of stator back-iron without diminishing output torque.

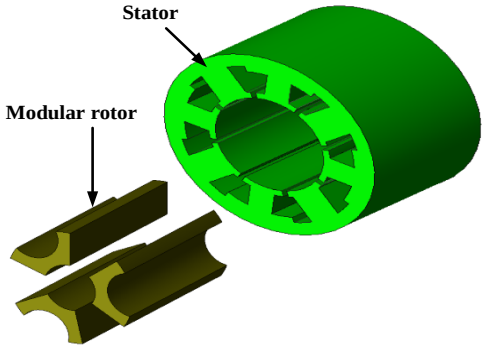

Figure 6. Modular rotor structure.

2. Design Methodology

The proposed novel modular rotor single phase eight-slot/six-pole FEFSM with non-overlapping winding arrangements is presented, as shown in Figure 7. To design the modular structure, JMAG designer ver.14.1 is used and the results obtained are validated by the 3D finite element analysis (3D-FEA). First, every section of motor such as stator, rotor, field excitation coil (FEC), and armature coil of modular design with eight stator slots and six rotor poles is designed in Geometry Editor. Then, the material, mesh properties, circuit, various properties, and conditions of the machine is selected and is simulated in the JMAG designer. The complete flow of the proposed design starts in Geometry Editor up to coil test analysis is shown in Figure 8. An electromagnetic steel sheet is used for the stator and rotor core. The design parameters and specifications of the modular design is illustrated in Table 1.

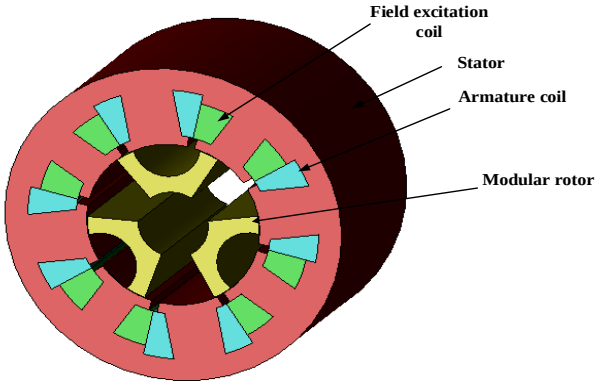

Figure 7. 8S-6P FEFSM with modular rotor.

Table 1. Design parameter of machines

Design Parameters	F1-A3-3P	Sub-Part Rotor Design	Modular Rotor Design
Number of phases	1	1	1
No. of slots	6	8	8
No. of pole	3	4	6
Stator outer diameter	96 mm	96 mm	96 mm
Rotor outer diameter	55.35 mm	53.55 mm	53.55 mm
Air-gap	0.45	0.45 mm	0.45 mm
Stator pole arc length	-	15.2 mm	5.5 mm
Teeth's arc of sub-rotor-1	-	15.2 mm	-
Teeth's arc of sub-rotor-2	-	26.9 mm	-
Rotor pole width	8 mm	-	5.6 mm
Stack length	60 mm	60 mm	60 mm
No. of turns per phase	120	30	30

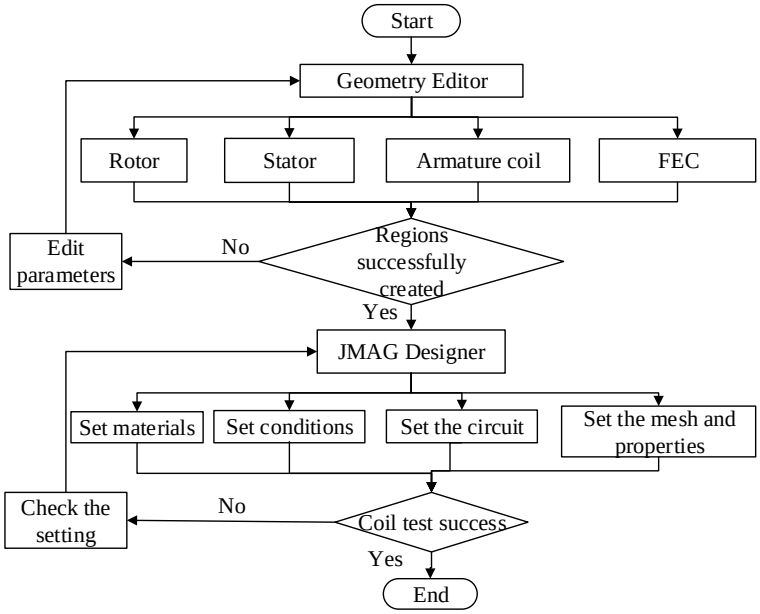

Figure 8. Design procedure.

3. Deterministic Optimization

The average torque analyses of eight-stator slots/six-rotor poles are examined. The maximum output torque obtained by the initial design is 0.88 Nm at speed of 400 rpm, which is much lower from the other designs. In order to improve the average torque characteristics, deterministic optimization is used. First optimization cycle consists of five steps, that is R_{IR}, θ, S_R, T_{WA}, T_{RA}, T_{WD}, and T_{RD}, as shown in Figure 9. Design free parameters R_{IR}, θ, S_R, T_{WA}, T_{RA}, T_{WD}, and T_{RD} are defined in rotor and stator part, as depicts in Figure 10 are optimized, while the outer radius of stator, air gap, and shaft of the motor are kept constant.

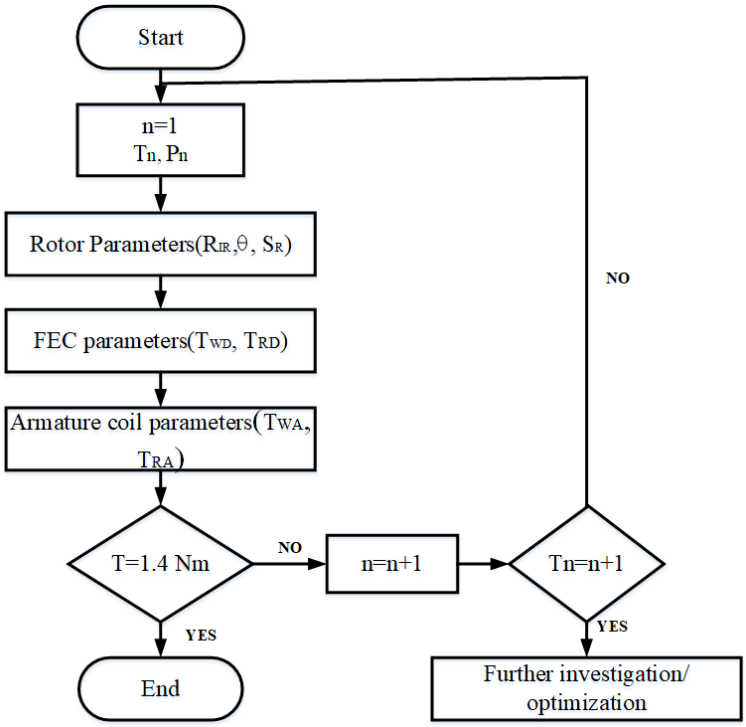

Figure 9. Optimization procedure.

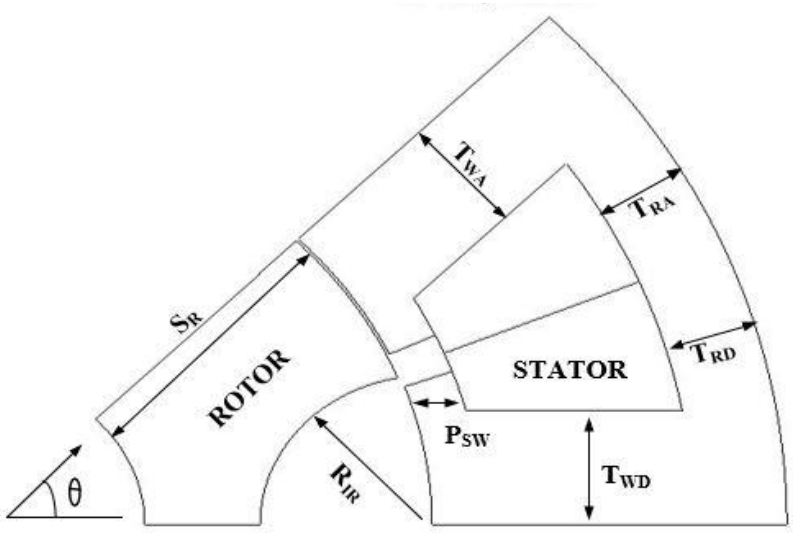

Figure 10. Design parameters of modular rotor design.

Initially, the design free parameters of rotor are updated, first of all, the inner rotor radius, R_{IR}, changes while the other parameters of stator and rotor remain constant. Then, rotor pole angle, θ, and split ratio, S_R, are varied and adjusted. The rotor pole angle, θ, is a dominant parameter in modular design to increase torque characteristics. Once the combination of promising values of rotor part for highest average output torque is determined, the next step is to refine the T_{WD} and T_{RD} of FEC, while rotor and armature slot parameter are kept constant. Finally, the essential armature slot is optimized by changing T_{WA} and T_{RA} while all other design parameters are preserved. To attain the highest average output torque, the above design optimization process is repeated. Figure 11 illustrates the highest average torque result after two cycles of optimization by updating several parameters that are already mentioned above. From Figure 11, it is also clear that during the first cycle the torque increases to a certain level by varying the above parameters of the machine and it becomes constant.

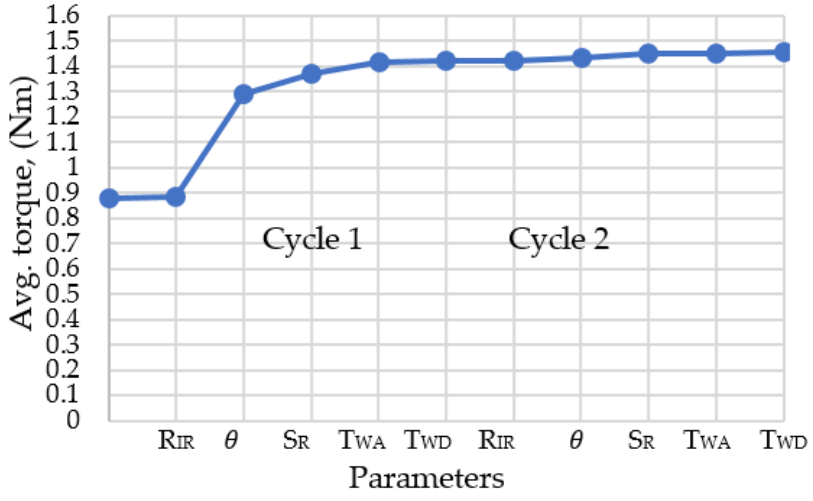

Figure 11. Effect of design parameters on average torque

During the first cycle, 32 percent of increase in the average output torque is achieved by refining the dominant parameter of rotor pole angle, θ, whilst other free design parameter adjustment shows less improvement in torque. In comparison with the initial design, the average output torque is improved by 40 percent after completion of second optimization cycle. The initial and optimized structure of

8S/6P modular design is illustrated in Figure 12. Additionally, the comparison of parameters of initial and final design is presented in Table 2.

Table 3 depicts comparison of cogging torque, flux linkage, back-EMF, average torque, and power of 3D-modular un-optimized and optimized design. The cogging torque and flux linkage of optimized designs is 0.3374 Nm and 0.2114 Wb respectively, which is 50% lower than the un-optimized cogging torque and flux linkage. Whilst, back-EMF of optimized modular 8S/4P is improved by 15%, that is still much lower than the applied input voltage of 220V. Furthermore, before optimization of modular design the maximum average output torque and power obtained is 9.77 Nm and 162.9 Watts respectively, at maximum FEC current density, J_e, is set to 10 A/mm^2 and 25 A/mm^2 is assigned to the armature coil, which is improved to 1.66 Nm and 288 Watts, respectively. Comparatively, average output torque and power is improved by 58.85% and 56.40%, respectively.

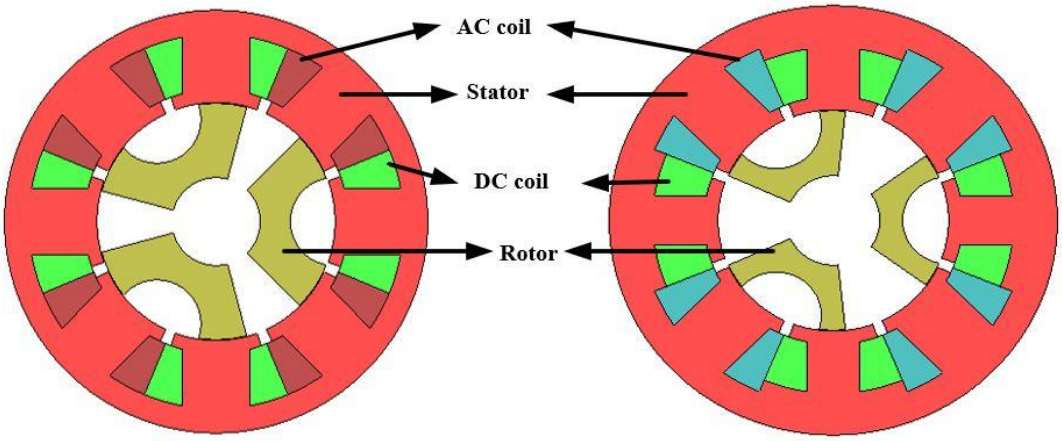

Figure 12. Structure of eight-slot/six-pole modular design.

Table 2. Initial and refined design parameters of Novel-modular rotor design

Parameters	Units	Initial Values	Optimized Values
Outer stator (OS)	mm	48	48
Inner stator (IS)	mm	27	24.7
Back-iron width of AC (T_{RA})	mm	42.5	41.4
Tooth width of AC (T_{WA})	mm	7.6	7.5
Back-iron width of DC (T_{RA})	mm	42.5	38.66
Tooth width of DC (T_{WD})	mm	7.6	5.5
Rotor inner circle radius (R_{IR})	mm	10	9.7
Pole shoe width (P_{SW})	mm	3	3
Rotor pole angle (θ)	deg	45	36
Split ratio (S_R)	-	0.55	0.5
Air gap	mm	0.45	0.45
Shaft radius	mm	10	10
Avg. torque	Nm	0.880	1.454

Table 3. Results comparison of optimized and un-optimized design

–	Cogging Torque (Nm)	Flux Linkage (Wb)	Back-EMF (Volt)	Avg. Torque (Nm)	Power (Watts)	Motor Mass (Kg)
Un-optimized design	0.67	0.01060	3.9	0.97775	162.986	4.02345
Optimized design	0.3374	0.02114	4.6	1.66148	288.967	3.84697

4. Result and Performance Based on 3D-FEA Finite Element Analysis (3D-FEA)

4.1. Flux Linkage

Comparison of flux linkages of three field excited FSM at no-load is examined by 3D-FEA [16,18]. To analyze the sinusoidal behavior of flux, the input current density of FEC, and armature coil is fixed to 10 A/mm^2 and 0 A/mm^2 respectively. Figure 13 shows that proposed modular design has peak flux of 0.021 Wb which is approximately equal to the peak flux of 15% of F1-A3-3P design. Similarly, sub-part rotor design has a 66% higher peak flux linkage than 8S/6P modular structure due to different pole arc length. The conventional F1-A3-3P design has the highest peak flux as compared to modular design, as well as sub-part rotor design due to the doubly salient structure.

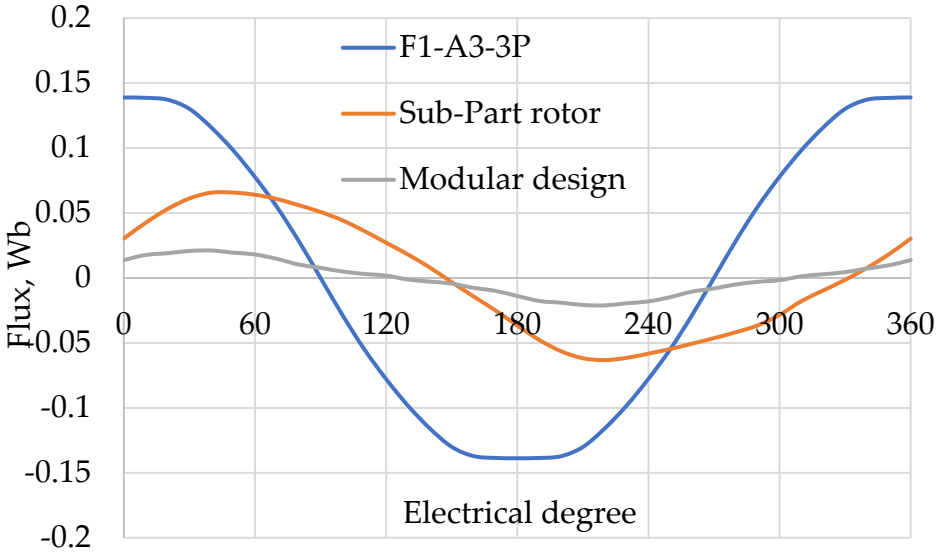

Figure 13. Comparison of U-flux linkages.

4.2. Flux Distribution

Flux density distribution generated by the DC coil in three FEFSM is shown in Figure 14. The red spot mention in Figure 14a–d show saturation of stator teeth and back-iron respectively of both conventional designs. F1-A3-3P design and sub-part rotor design has vector plot value of magnetic flux density distribution of 1.9953 and 1.9760 maximum, respectively. Whilst, the flux density distribution of modular design from the vector plot is 2.2528 maximum at 0° rotor position. Additionally, in comparison with 8S/4P sub-part rotor design and 6S/3P design, the proposed 8S/6P modular rotor design exhibits higher flux distribution. For completely utilizing flux in the proposed design, various parameters of the machine are optimized to enhance the flux distribution from the stator to the rotor and vice versa. The peak flux in the modular rotor pole at its lowest magnetic loading is 0.0453 Wb, which increases with increasing magnetic loading. Figure 15 illustrates flux density distribution at maximum armature current density of 25 A/mm^2.

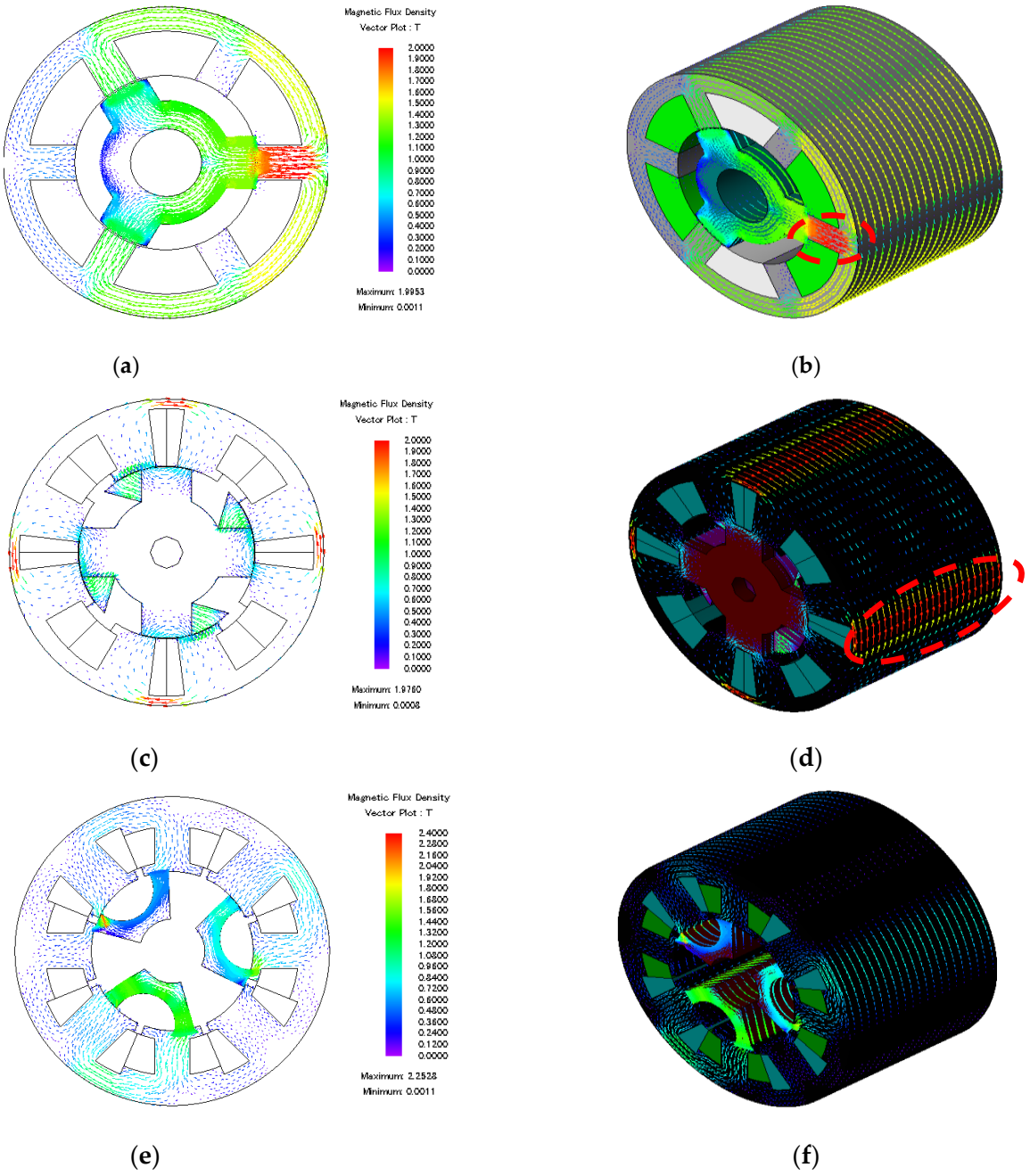

Figure 14. Flux distribution at no-load. (**a**,**b**) Flux distribution in conventional F1-A3-3P design; (**c**,**d**) Flux distribution in sub-part rotor design; (**e**,**f**) Flux distribution in proposed modular rotor design.

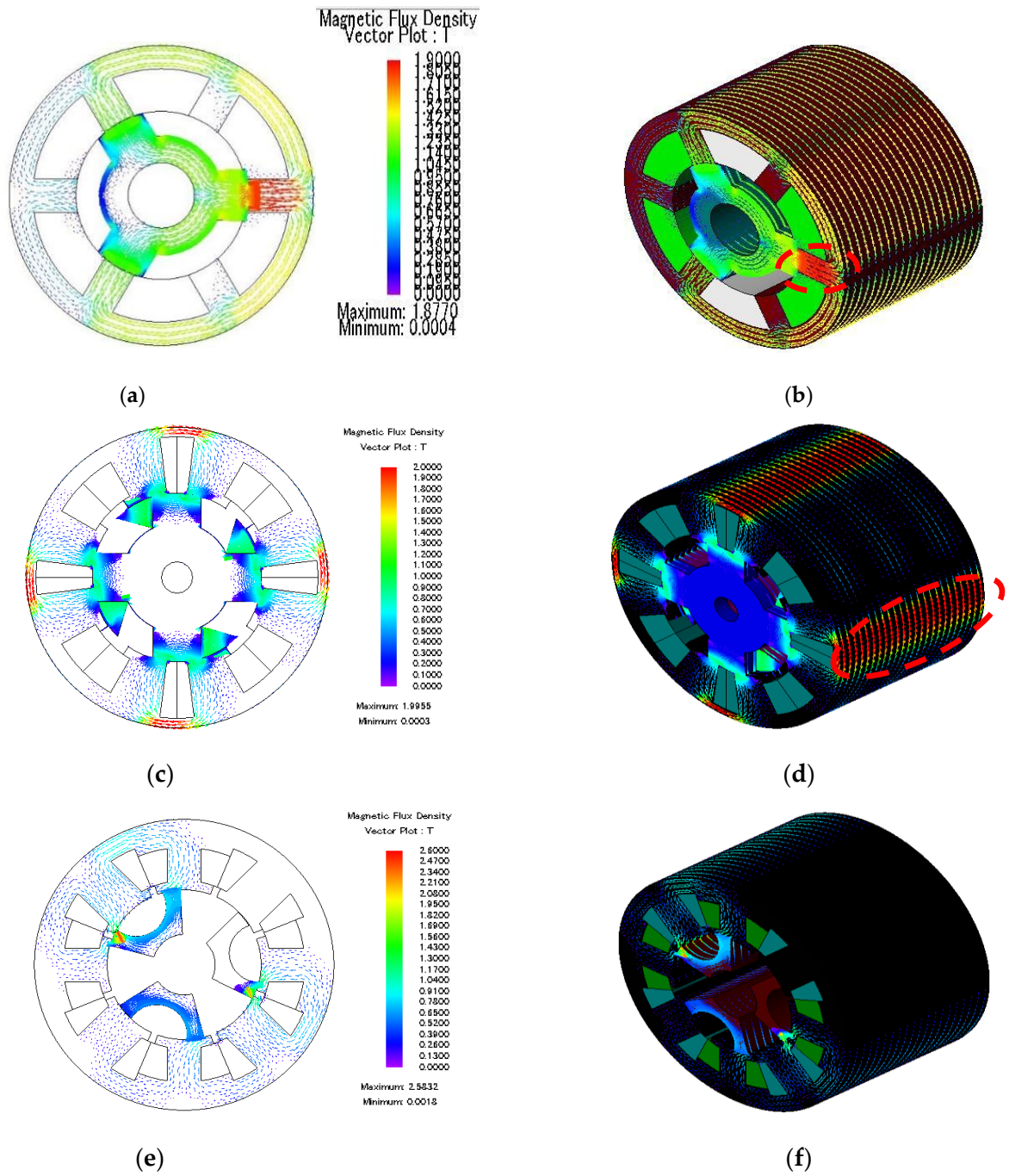

Figure 15. Flux distribution at maximum load. (**a**,**b**) Flux distribution in conventional F1-A3-3P design; (**c**,**d**) Flux distribution in sub-part rotor design; (**e**,**f**) Flux distribution in proposed modular rotor design.

4.3. Flux Strengthening

The effect of flux strength is analyzed by increasing current density; J_e of field excitation coil (FEC) is varied from 0 A/mm^2 to 20 A/mm^2, whilst armature current density; J_a is set 0 A/mm^2. The FEC input current is calculated from (1)

$$I_e = \frac{J_e \alpha S_e}{N_e} \tag{1}$$

where, I_e, J_e, α, S_e, and N_e are the input current of FEC, field current density, filling factor, slot area of FEC, and number of turns of field coil respectively. The analysis of coil test can be verified from

the flux strengthening. Increasing the current densities of FEC, the pattern plot clearly shows a linear increase in flux until 0.027 Wb at J_e of 20 A/mm^2 as shown in Figure 16.

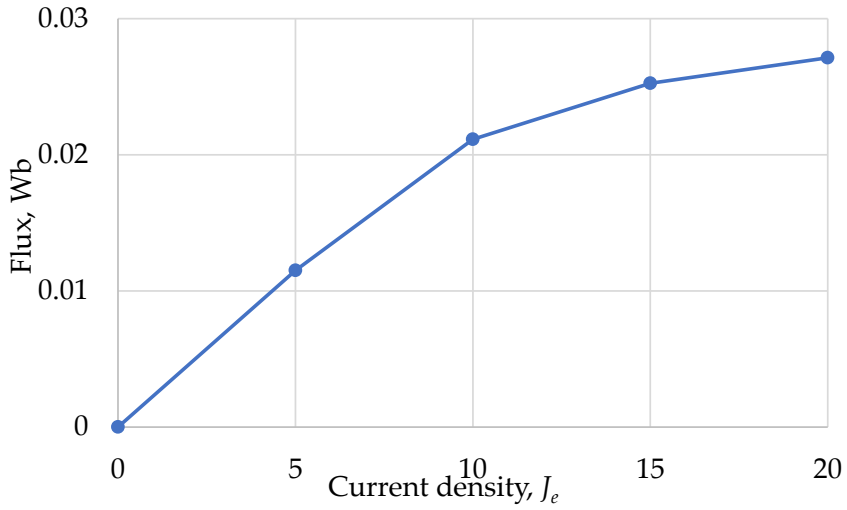

Figure 16. Peak flux strengthening with Modular rotor at various J_e.

4.4. Back-EMF Versus Speed

"Back-EMF is the induce voltages in the armature winding which opposes the change in current through which it is induced". The back-EMF (e_a) in the armature can be determined from the rate of change in armature flux or applying the co-energy concept [19]. For motor with N_r rotor poles

$$e_a = \omega \phi_f \frac{2KN_aN_r}{\pi} \tag{2}$$

where N_a, N_r, ω, ϕ_f and K is number of armature turns, number of rotor poles, rotational speed, field flux, and constant of field flux that are linked with the armature winding respectively. Substituting the ϕ_f (field flux) with

$$\phi_f = \frac{N_f I_f}{\mathcal{R}} \tag{3}$$

$$e_a = \frac{2KN_r}{\pi \mathcal{R}} N_a N_f I_f \omega \tag{4}$$

where N_f, I_f, and $\mathcal{R}$ is the number of field turns, the field current and reluctance of magnetic circuit. For the maximum conversion of electro-mechanical energy, armature current must flow in the opposite direction of the induced-EMF in the armature.

Figure 17 shows the 3D-FEA predicted induced-EMF of eight-slot/six-pole modular rotor structure at a fixed field current density (J_e; 10 A/mm^2) and various speeds. The induced-EMF increases linearly with increasing speed. The maximum induced voltage is 22 V at a maximum speed of 1600 rpm which is quite lower than the applied input voltage (220 V) which confirms the motor actioning of the machine.

4.5. Intantaneous Torque and Torque Ripple Calculation

Figure 18, investigates the instantaneous torque versus rotor mechanical revolution in electrical degrees of eight-slot/four-pole, six-slot/three-pole, and eight-slot/six-pole FESF machines. Six-slot/three-pole (F1-A3-3P) rotor design has high peak to peak torque as compared to eight-slot/six-pole (modular design) and eight-slot/four-pole (sub-part rotor) FESF machines. Figure 18 illustrates that characteristics of instantaneous torque at 10 A/mm^2 of six-slot/three-pole are better as compared to eight-slot/six-pole and eight-slot/four-pole FESF machines.

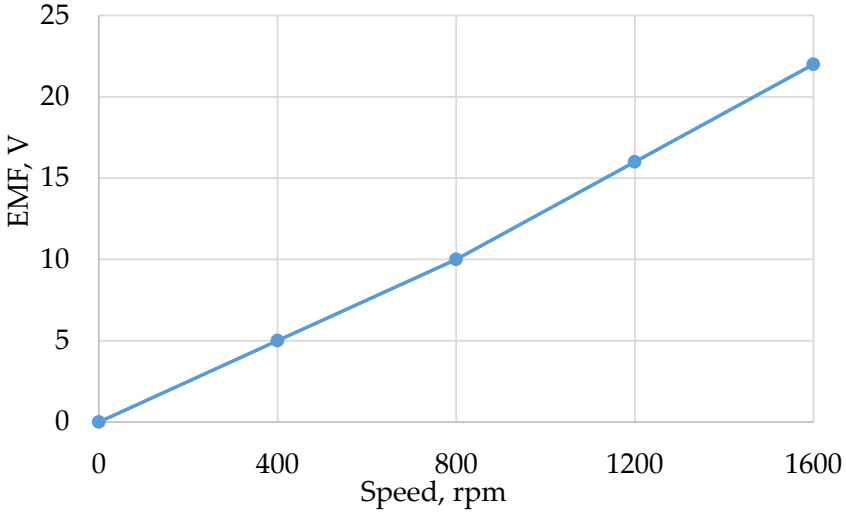

Figure 17. Maximum back-EMF at various speed.

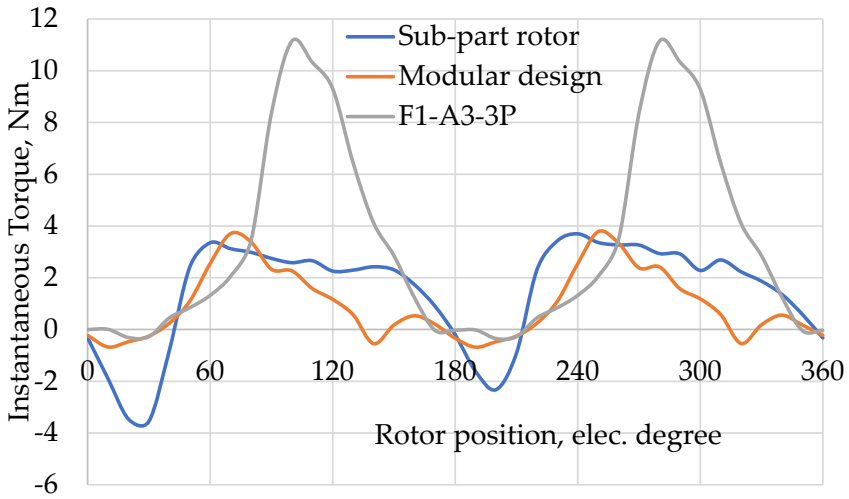

Figure 18. Comparison of instantaneous torque.

Whilst F1-A3-3P design exhibits the highest torque ripples comparatively to sub-part rotor design and modular rotor design. The proposed modular design has lower torque ripples than both the conventional designs, that is 29% and 60% lower than sub-part rotor design and F1-A3-3P design, respectively. Torque ripples are calculated from expression (5)

$$\left(\frac{\tau_{max} - \tau_{min}}{\tau_{avg}}\right) \times 100 \tag{5}$$

4.6. Total Harmonics Distortion (THD)

Total harmonics distortion is the ratio of the summation of all harmonic components to the fundamental frequency harmonics of the power or harmonics distortion that exists in flux. In electric machines, THD occurs due to harmonics present in flux. THD determines the electromagnetic performance of the machine as it is the representation of the harmonics in the machine. Mathematically, the THD of an electric machine can derived from equation (6)

$$THD = \frac{\sqrt{\sum_{n=1,2\ldots}^{k=2n+1} \Phi_k^2}}{\Phi_1} \tag{6}$$

where k is odd number and Φ_k is the odd harmonics of flux. THD of proposed design is higher as compared to conventional design due to the modular structure of rotor. Figure 19 shows the THD of three FEFS machines. The graph shows that the THD of sub-part rotor design and F1-A3-3P design is 7% and 4% respectively, while THD of the proposed modular rotor design is 16.4%.

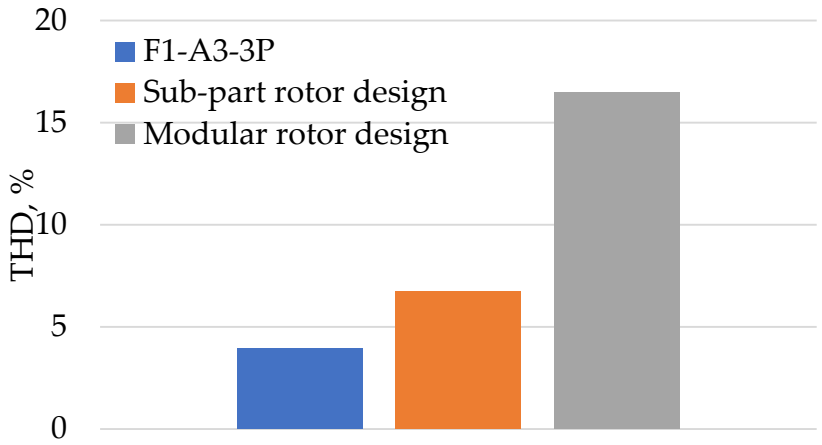

Figure 19. THD values of the conventional and proposed designs.

4.7. Cogging Torque

The interaction between the Stator excitation source (PM, excitation coil) and rotor pole of machine at no-load is called cogging torque. The magnetic circuit consists of an existing PM and coil having co-energy, the total co-energy is formulated as [20,21].

$$W_c = Ni\varphi_m + \frac{1}{2}\left(Li^2 + (\mathcal{R} + \mathcal{R}_m){\varphi_m}^2\right) \tag{7}$$

where, N, i, $\mathcal{R}_m$, L, $\mathcal{R}$ and φ_m are the number of turns, current, magnetic flux, inductance of coil, magneto-motive force, and magnetic flux linkage respectively. The change in total co-energy with respect to the mechanical angle of the rotor determines the average torque of the machine.

$$T_e = \frac{\partial W_c}{\partial \theta} \; with \; i = constant \tag{8}$$

where, W_c and θ are total co-energy and mechanical rotor angle, respectively.

$$T_e = \frac{\partial\left(Ni\varphi_m + \frac{1}{2}\left(Li^2 + (\mathcal{R} + \mathcal{R}_m){\varphi_m}^2\right)\right)}{\partial\theta} \quad T_e = Ni\frac{d\varphi_m}{d\theta} + \frac{1}{2}i^2\frac{dL}{d\theta} - \frac{1}{2}{\varphi_m}^2\frac{d\mathcal{R}}{d\theta} \tag{9}$$

The third term in Equation (9) changes in mmf with respect to the mechanical position of rotor causes cogging torque. The cogging torque produces unwanted noise and vibration. As Equation (9) shows that the cogging torque lead to a significant reduction in the average torque.

The cogging torque of F1-A3-3P, sub-part rotor and modular designs is comparing in Figure 16. The cogging of modular design is less than F1-A3-3P and sub-part rotor designs as depicts in Figure 16. Figure 20 illustrates that the cogging torque of modular design is 12% of F1-A3-3P and 53% of sub-part rotor. As a result, the modular design has less vibration and more average torque as to compare to F1-A3-3P and sub-part rotor design.

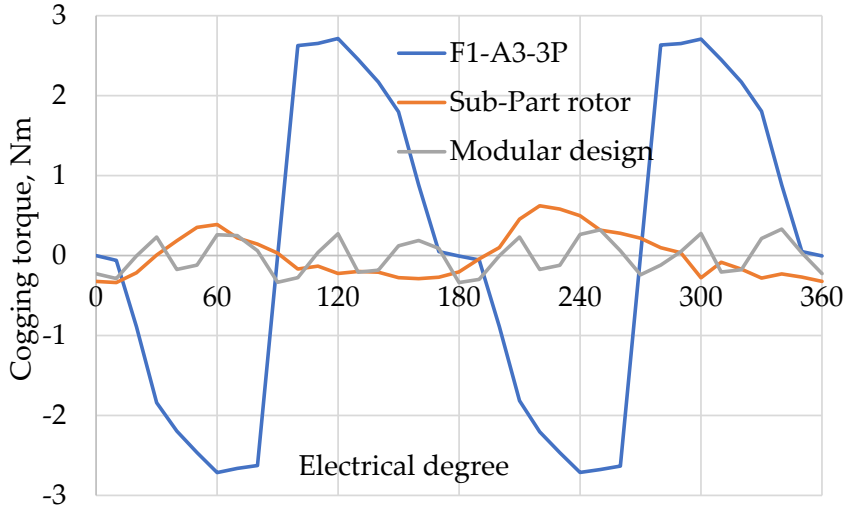

Figure 20. Comparison of cogging torque.

4.8. Copper Loss versus Torque

In field excited FSM, the copper consumption is the main constituent affecting the overall cost of the machine. As compared to other materials for FEFSM, copper is more expensive. The copper-loss of single phase FEFSM can be calculated from the formula as

$$P_{Cu} = I_a^2 R_a + I_f^2 R_f$$

where I_a, R_a, I_f, and R_f is the armature current, armature winding resistance, field current, field winding resistance, respectively. The comparison of copper loss-torque curve of three field excited FSM is shown in Figure 21. The average output torque modular design is almost similar to the sub-part rotor design but is much higher than the F1-A3-3P design. At fixed copper loss of 60 watts, the average torque of conventional sub-part rotor design, F1-A3-3P design, and proposed modular design is 1.6 Nm, 0.98 Nm, and 1.58 Nm, respectively. However, the plot clearly shows that modular design achieves a higher average torque under the constraint of maximum copper loss of 120 watts due to the short pitch coils.

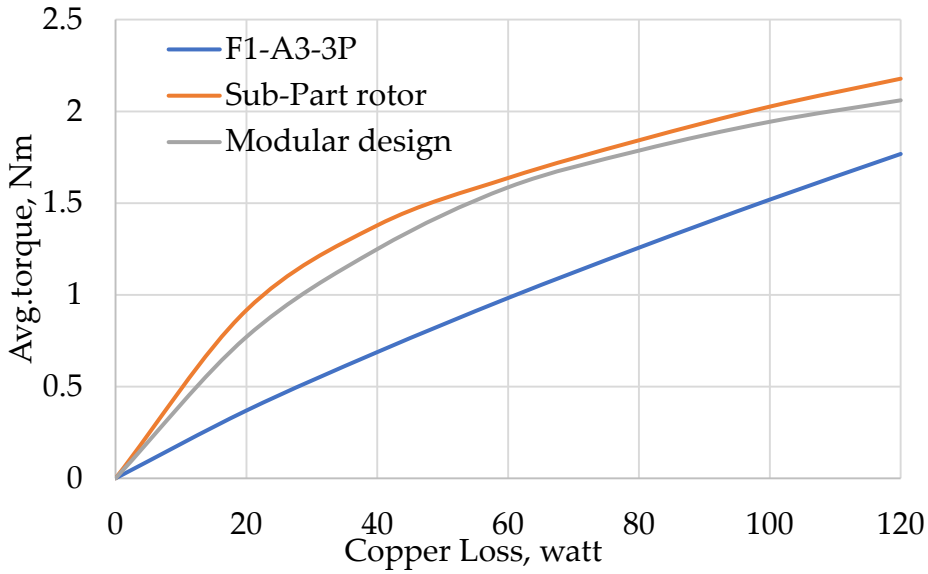

Figure 21. Comparison of average torque at fixed copper losses.

4.9. Torque versus Current Density

Torque versus current density of three FEFS machines is calculated at various current density and maximum current set to 25 A/mm^2. Figure 22 illustrates torque versus the current density of sub-part rotor design, F1-A3-3P design, and modular rotor design. Both conventional machines are saturated beyond 10 A/mm^2, while proposed machine has increasing torque profile, by increasing current density. At maximum 25 A/mm^2 current density F1-A3-3P design has higher average torque than modular rotor and sub-part rotor 65.6% and 63.05%, respectively. F1-A3-3P demonstrates high torque due to high flux linkage.

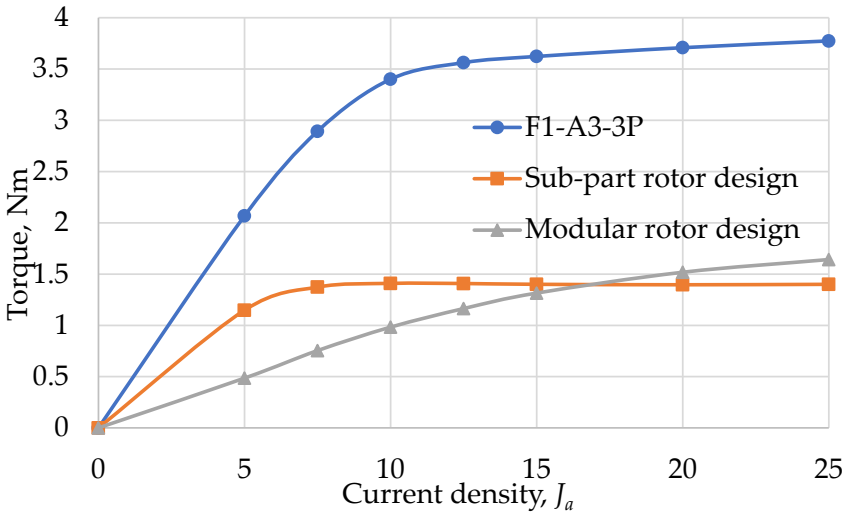

Figure 22. Comparison of average torque versus current densities.

4.10. Torque Density and Power Density

Torque density and power density of three FEFS machines is calculated at a fixed current density of 10 A/mm^2. Figure 23 illustrates torque densities of sub-part rotor design, F1-A3-3P design, and modular rotor design. Comparatively, the torque density of the F1-A3-3P design is 1.89 times higher than modular rotor design and 1.71 times higher than sub-part rotor design as shown in Figure 23. The proposed modular design has a reduced total mass of 23% and 44.8% as compared to sub-part rotor design and F1-A3-3P design, respectively, as shown in Table 4.

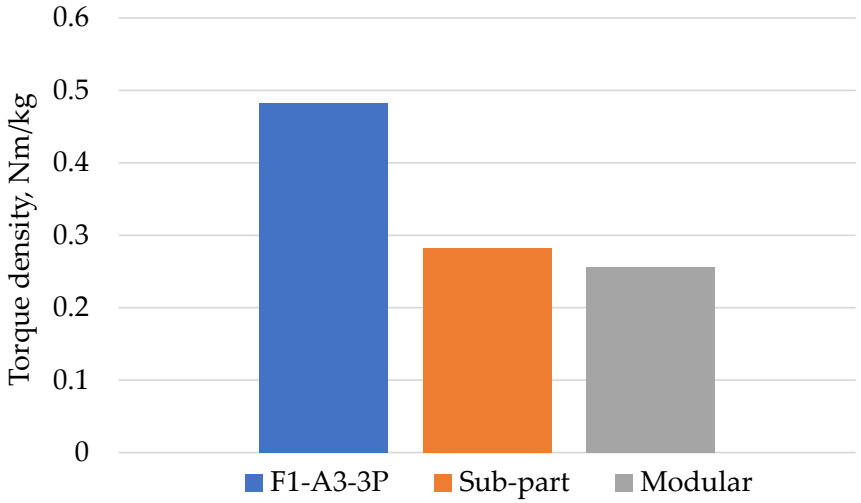

Figure 23. Torque density of three FEFS machines.

Table 4. Comparison of active mass

Design	Stator Mass (Kg)	Rotor Mass (Kg)	Copper Mass (Kg)	Total Mass (Kg)
F1-A3-3P	1.366	0.536	5.137	7.04
Sub-part rotor design	1.499	0.732	2.758	4.99
Modular rotor design	1.825	0.247	1.774	3.84

The power density of conventional and proposed design is expressed in Figure 24. Power density attains by modular rotor design is 0.0783 Watt/kg at current density of FEC, J_e, and armature current density, J_a, of 10 A/mm^2 as shown in Figure 24. High power density exhibits high efficiency and better electromagnetic performance. The proposed 8S/4P modular rotor design achieves 1.3 times and 1.9 times higher power densities as compared to F1-A3-3P design and sub-part rotor design respectively.

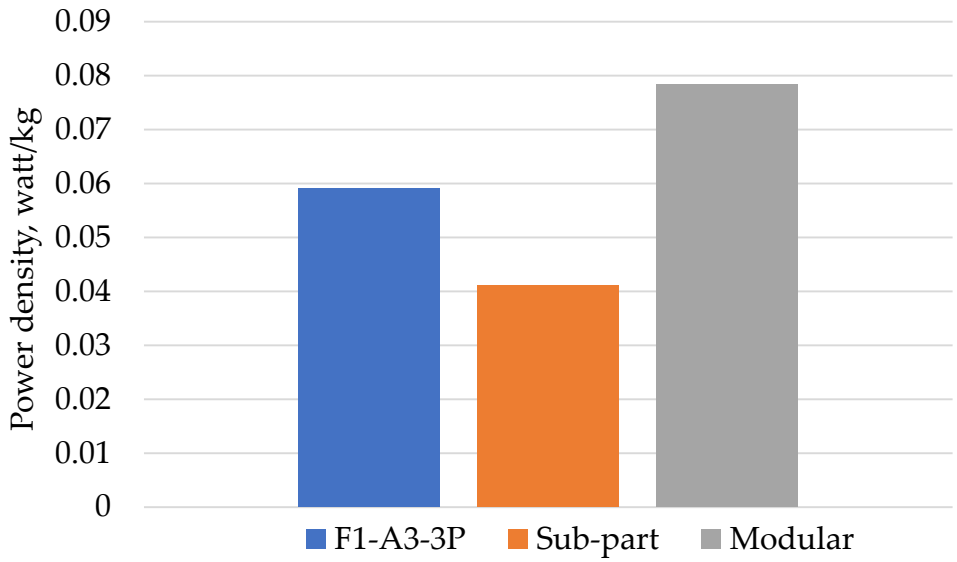

Figure 24. Power density of three FEFS machines.

4.11. Torque and Power Versus Speed Characteristics

The comparison of torque and power versus speed curve of three single phase FEFSM are illustrated in Figure 25. At a rated speed of 1664 rpm, the maximum average torque of the modular rotor design is 1.64 Nm which corresponds to the power generated by the proposed design at 286 W. Additionally, the average torque obtained by conventional 8S-4P sub part rotor design and 6S-3P salient rotor is 1.4 Nm and 3.77 Nm, at a base speed of 1389 rpm and 1053 rpm, respectively. The average torque of proposed design is higher as compared to the sub part rotor design. At a speed of 1600 rpm, the average torque of the proposed design is similar to 6S-3P design while being 19 percent higher than the 8S-4P design. Although the generated power of 8S-6P modular design is 28.4 percent higher than 8S-4P design, it is 31 percent lower than F1-A3-3P design. The pattern plot shows that, beyond rated speed, the average torque of the machine starts to decrease and power is decreased as well. The power of 6S-3P FEFSM decreases more rapidly due to an increase in iron loss above the rated speed.

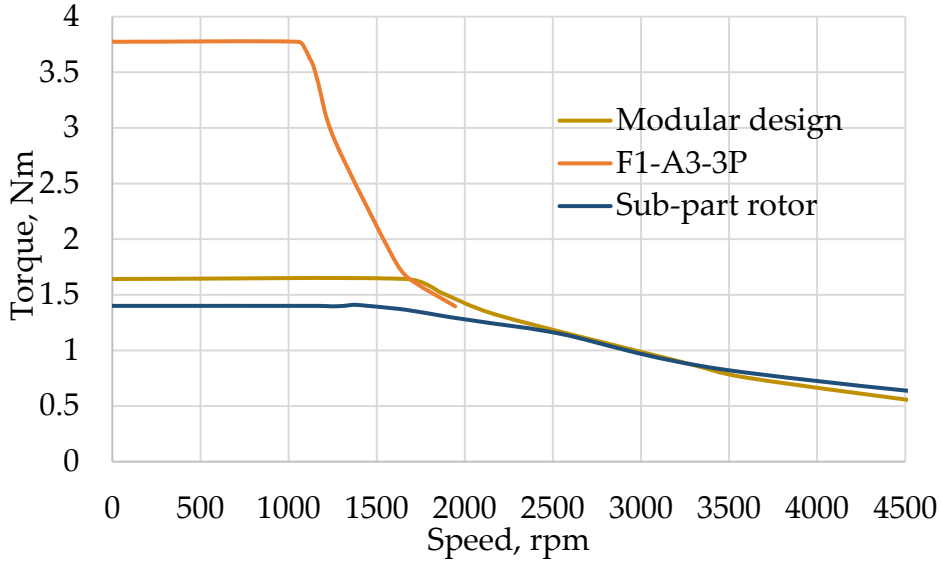

(**a**)

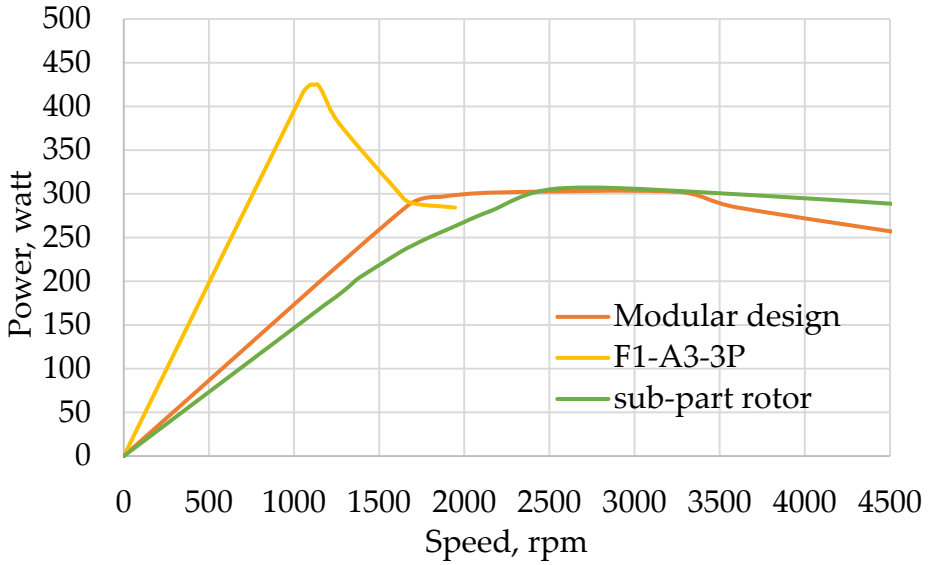

(**b**)

Figure 25. (**a**) Comparison of torque versus speed; (**b**) Comparison of power versus speed of three FEFSM.

4.12. Rotor Stress versus Speed

Rotor stress analysis is a technique to identify the principal stress, nodal force, and displacement occurred in the rotor structure in an ideal state after load is applied. Generally, the condition for mechanical stress of the rotor structure is accomplished by centrifugal force due to the longitudinal rotation of the rotor. Additionally, centrifugal force of the rotor is greatly affected by the speed. The rotor could highly withstand stress, if the principal stress of the rotor is higher. Principal stress is a crucial result in the analysis of stress. By increasing the angular velocity of the rotor, principal stress is increased exponentially. Thus, the rotor principal stress versus the speed of the three-field excited flux switching machines (rotor structure) is analyzed using 3D-FEA. The angular velocity varies from 0 rpm to 20,000 rpm for conventional three-pole salient rotor structure, four-pole sub-part rotor structure, and the proposed six-pole modular structure to analyze the maximum capability of

mechanical stress. The constraints that coincide with the force acting on the rotor is faces, edges, and vertices. The maximum principal stress on each rotor at various speed is shown in Table 5.

Table 5. Stress analysis at various speed

Speed	5000	20,000
F1-A3-3P	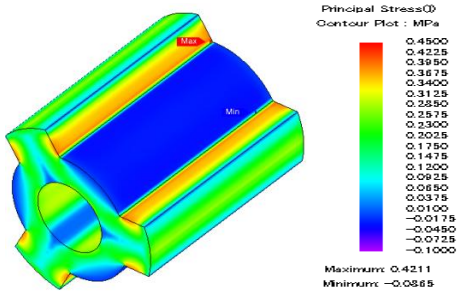	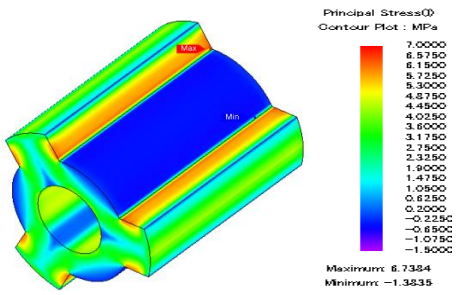
	(a)	(b)
Sub-part Rotor Design	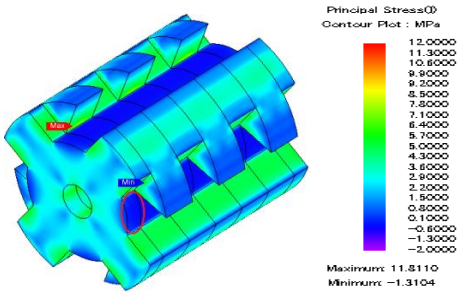	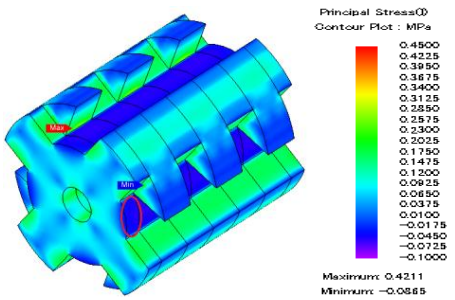
	(c)	(d)
Modular rotor design	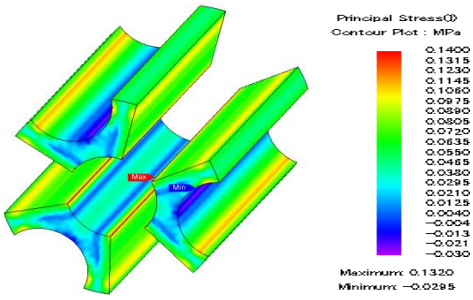	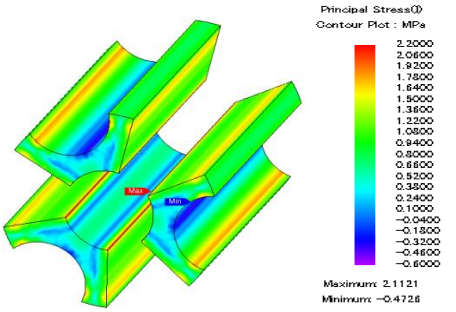
	(e)	(f)

Figure 26 shows that comparison of principal stress of three different rotor structures versus speed. At a maximum speed of 20,000 rpm, the principal stress of salient rotor structure, sub-part rotor structure and modular rotor structure is 6.73 MPa, 11.61 MPa, and 2.11 MPa respectively. The pattern plot clearly shows that principal stress of proposed modular rotor structure is much lower as compared to the conventional rotor design. The maximum allowable principal stress of 35H210 electromagnetic steel is 300 MPa. All the three rotor structures are capable of high-speed applications, but the only salient rotor structure can be operated at high speeds due to the single piece rotor structure. Whilst the sub-part rotor and modular structure are only applicable for low-speed applications.

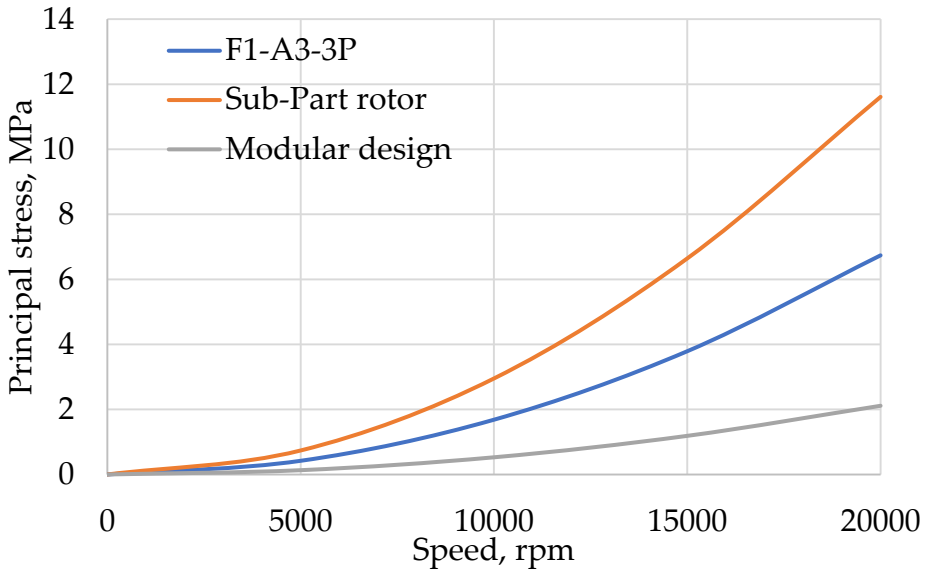

Figure 26. Principal stress against speed.

4.13. Copper Losses versus Je at Various Ja

Copper losses of three FEFSM at various armature current densities is shown in Figure 27. To analyze the total copper losses, FEC current density, J_e, is set to 10 A/mm^2, and armature current density is varied from 0 A/mm^2 to 25 A/mm^2. Figures 28–30, illustrate copper losses of both armature coil and FEC, in isolation at fixed J_e, whilst J_a changes to maximum. The pattern plot clearly showed that the copper losses are increased with increasing current densities. Comparatively, the proposed modular rotor design shows approximately 56% and 88% lower copper losses to sub-part rotor design and F1-A3-3P design respectively, at a maximum armature current density of 25 A/mm^2 as depicted in Figure 27. However, the proposed structure has reduced copper losses, indicating improved efficiency compared with the conventional designs.

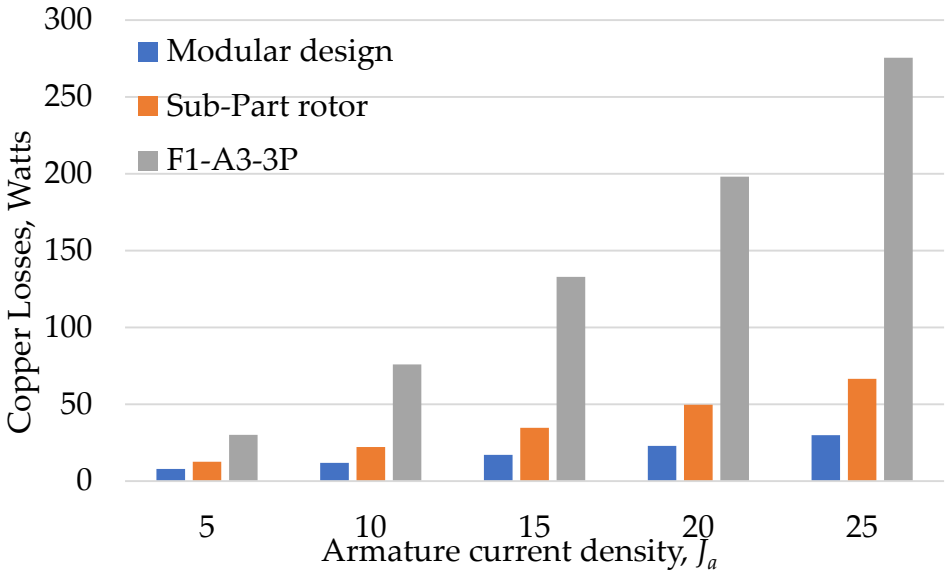

Figure 27. Copper losses versus various J_a.

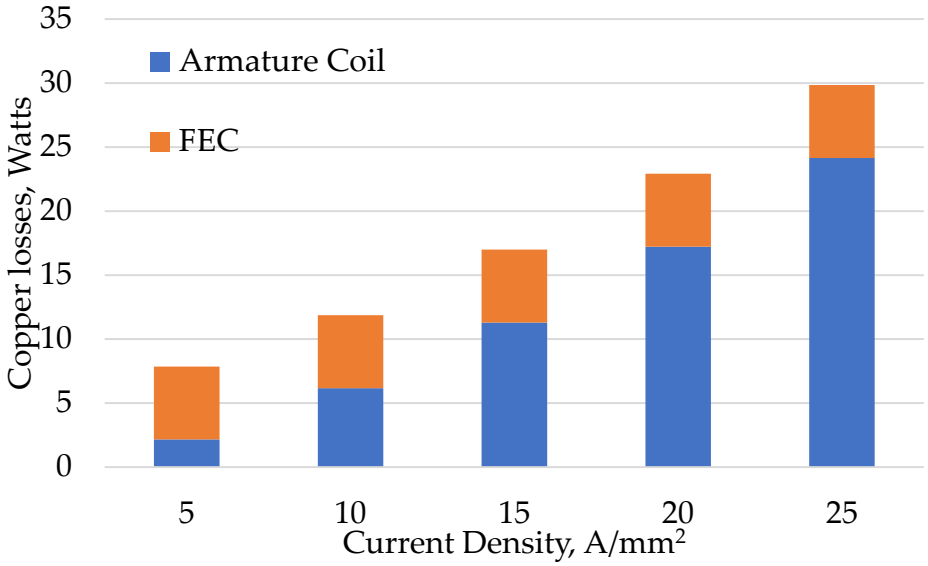

Figure 28. Copper losses of modular rotor design.

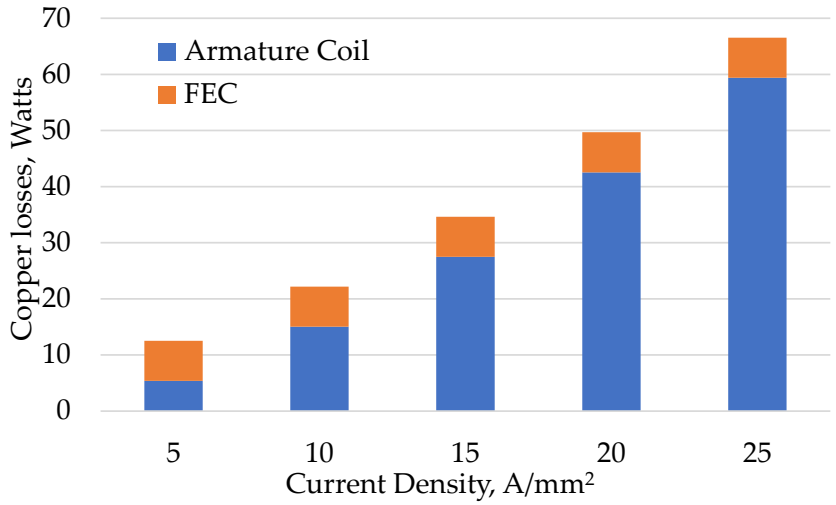

Figure 29. Copper losses of sub-part rotor design.

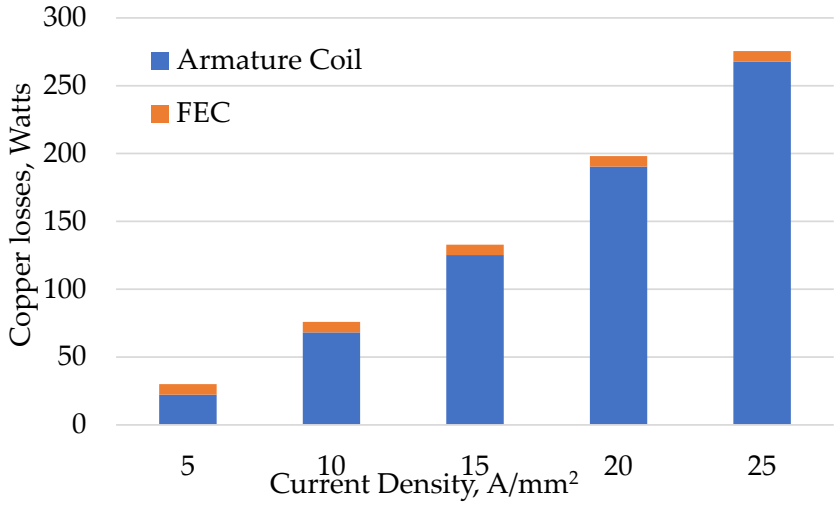

Figure 30. Copper losses of F1-A3-3P design.

4.14. Iron Loss versus Speed

Iron loss is a significant portion in the total losses of machine. Machine performance is greatly affected by iron losses due to flux emphasis of novel-modular topology in the stator, which generates a variation of flux densities in the rotor and stator core [17,22]. The flux density variation is expected to be reduced by implementing the novel-modular topology due to the reduction in utilization of the stator. Iron losses are increased with increasing electrical loading due to higher armature reaction [23]. The iron losses of the switched flux machine also vary greatly with speed at every part as shown in Figures 31–33. At low-speed, the machine dominates electromagnetic losses. The method of iron loss calculation can be found in [17,24].

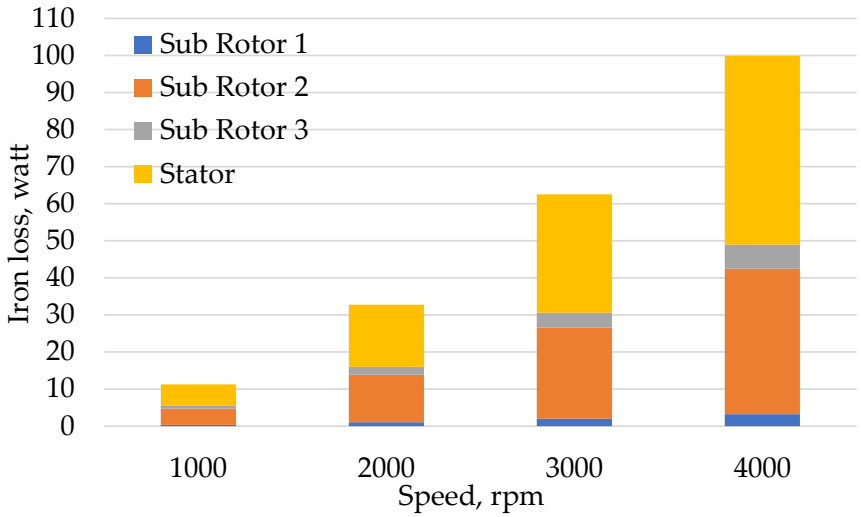

Figure 31. Iron loss at various parts of sub-part rotor design.

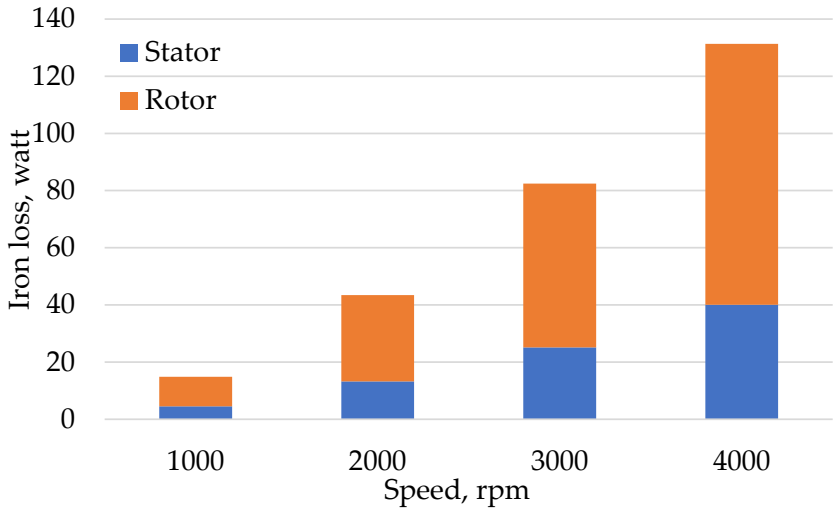

Figure 32. Iron loss at stator and rotor part of F1-A3-3P design.

The iron loss of each component of three-field excited FSM is calculated by 3D-FEA. In Figure 34, the plot clearly shows that the proposed modular rotor structure has lowest iron loss then the conventional sub-part rotor design and F1-A3-3P design. At a maximum speed of 4000 rpm, modular design reduces the iron losses of 29.44% and 7.22% compared with the conventional F1-A3-3P design and sub-part rotor design respectively. The reason for iron loss reduction in the stator is due to the modular rotor, variation of flux densities in the stator-core is investigated in [25].

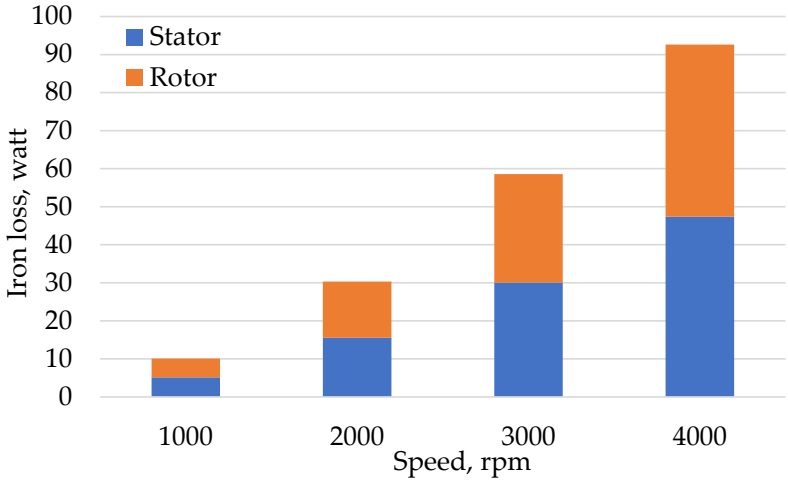

Figure 33. Iron loss at stator and rotor part of modular rotor design.

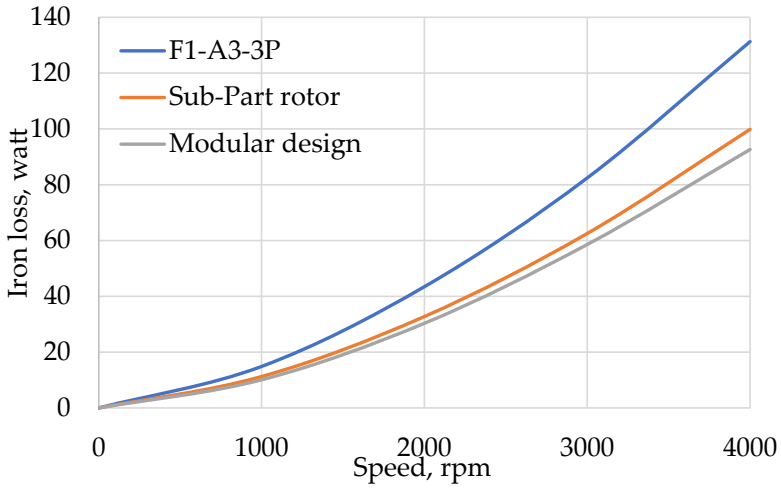

Figure 34. Comparison of iron losses at various speeds.

4.15. Motor Losses and Efficiency Analysis

The efficiencies of three FEFSMs are computed by 3D-FEA, considering all motor losses (iron losses in core laminations and copper losses in FEC and armature coil). Copper losses (P_{cu}) are calculated at fixed current densities of 10 A/mm^2, for both *FEC*, J_e, and armature coil, J_a, for all designs. Whilst, the iron losses are calculated at varying speed of 1000–4000 rpm. In single phase FEFS machines, copper losses can be illustrated as

$$P_{Cu} = I_a^2 R_a + I_f^2 R_f \quad (10)$$

where P_{cu}, I_f, R_f, I_a, and R_a are copper losses, field current, total field coil resistance, armature current, and total armature coil resistance, respectively. Figure 35a–c shows iron losses (P_i), copper losses (P_{cu}), output power (P_o), and efficiency at different speeds (range: 1000–4000 rpm) of sub-part rotor design, F1-A3-3P design, and modular rotor design, respectively. However, with increasing speed the iron losses increase in addition to further degrading efficiency. Furthermore, at every operating speed from 1000 rpm to 4000 rpm, the proposed design achieves comparatively higher efficiencies. At a max speed of 4000 rpm, the iron losses of the proposed modular rotor design are 9% and 30% lower than the conventional sub-part rotor design and F1-A3-3P design, respectively. However, reduction in iron losses shows a significant reduction in total machine losses, approximately 49% of F1-A3-3P design and 15% of sub-part rotor design. Furthermore, by adopting the modular structure, the proposed 8S/6P design achieves a higher average efficiency of approximately 12.8% and 11.4% higher than the

conventional F1-A3-3P and sub-part rotor designs, respectively. Finally, it can be seen from Figure 36 that the efficiency of a single phase modular 8S/4P FEFS machine exhibit higher efficiency than other conventional FEFS machines.

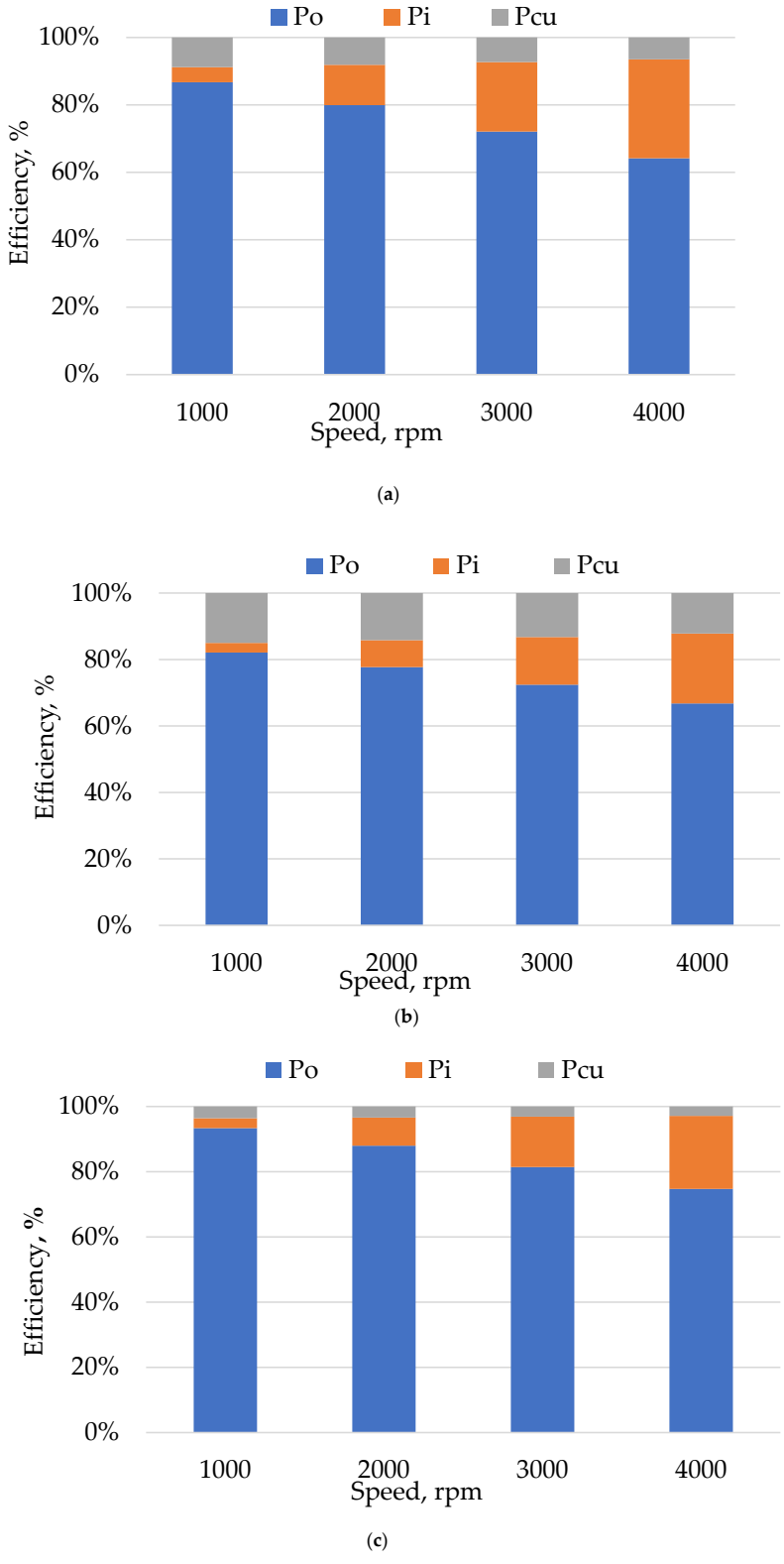

Figure 35. (**a**) Losses and efficiency of sub-part rotor design at various speeds. (**b**) Losses and efficiency of F1-A3-3P design at various speeds. (**c**) Losses and efficiency of modular rotor design at various speeds.

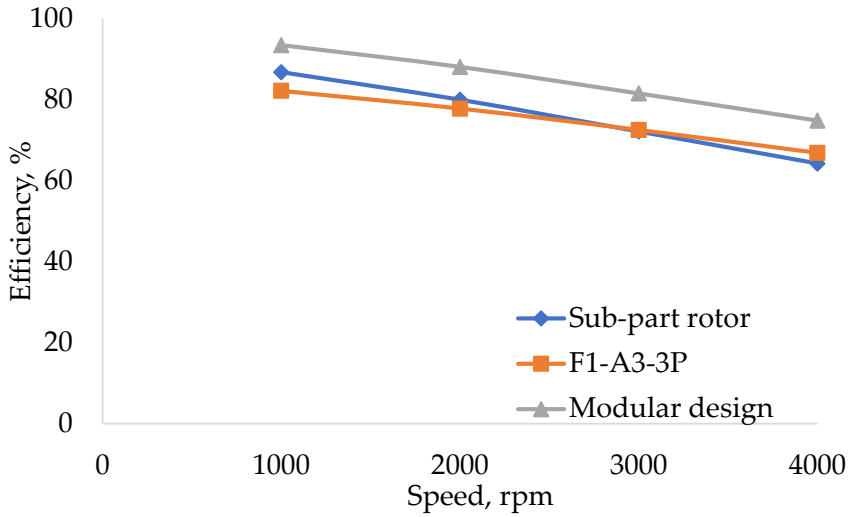

Figure 36. Comparison of efficiency at various rotor speeds.

5. Conclusions

A novel single-phase field excited topology of modular rotor flux switching machine is presented and the result is investigated by 3D-FEA.

In this paper, a comparison of single-phase eight-slot/four-pole sub rotor design and six-slot/three-pole salient rotor design with a novel modular rotor eight-slot/six-pole FSM is demonstrated. For comparison of flux linkage, cogging torque, average torque, and other different analyses of proposed FEFSMs, an optimal split ratio is set identical to the conventional designs.

The performance comparison of the three different types of single-phase eight-slot/four-pole sub rotor design and six-slot/three-pole salient rotor designs with a novel modular rotor eight-slot/six-pole FSM is demonstrated. he optimal split ratio is kept the same as the conventional designs for comparison of flux linkage, cogging torque, average torque, and other analyses of the proposed FSM. The initial design achieved inadequate power and torque production. Therefore, a deterministic optimization technique was adopted to improve the characteristics. The optimized design enhanced power, torque, and efficiency compared to existing eight-slot/four-pole and six-slot/three-pole FESF machines.

Novel modular 8S/6P single phase FSM with non-overlapped winding arrangement is designed. Copper consumption of modular rotor design is much lower than conventional designs that is 90% lower than F1-A3-3P and 56% than sub-part rotor design, at J_a = 25 A/mm^2, due to non-overlap winding between FEC and armature coil. The proposed design shows a higher average output torque when compared under constraints of fixed copper losses. Modular rotor structure also exhibits a significant reduction in iron losses, 30% as compared to F1-A3-3P and 9% reduced when compared with sub-part rotor design. Due to the modular structure of the rotor, the active rotor mass of the proposed design is reduced and the use of stator back-iron is lowered without diminishing torque output. This research also examines the principal rotor stress of the conventional rotor designs (sub-part rotor design and three-pole salient rotor design) and proposed (modular) rotor design with a different direction of constraints. Additionally, average efficiency of proposed modular design is increased by 12.8% compared with F1-A3-3P design and 11.4% compared with sub-part rotor design. Hence, the proposed motor is suitable for pedestal fan application by replacing induction machine. The proposed design has not yet been comprehensively analyzed and will be examined in our future work.

Author Contributions: Conceptualization, L.U.R. and F.K.; methodology, M.S.; software, H.A.K.; validation, N.A., L.U.R.; investigation, L.U.R.; resources, F.K.; data curation, H.A.K.; writing—original draft preparation, L.U.R.; writing—review and editing, L.U.R.; visualization, S.A.; supervision, F.K.; project administration, M.A.K.; funding acquisition, L.U.R., F.K., and H.A.

Funding: There is no external funding.

Acknowledgments: This work was supported by COMSATS University Islamabad, Abbottabad Campus and Higher Education Commission of Pakistan (No 8114/KPK/NRPU/R&D/HEC/2017).

Conflicts of Interest: The authors declare no conflict of interest.

References

1. You, Z.C.; Yang, S.M.; Yu, C.W.; Lee, Y.H.; Yang, S.C. Design of a High Starting Torque Single-Phase DC-Excited Flux Switching Machine. *IEEE Trans. Ind. Electron.* **2017**, *64*, 9905–9913. [CrossRef]
2. Fernando, N.; Nutkani, I.U.; Saha, S.; Niakinezhad, M. Flux switching machines: A review on design and applications. In Proceedings of the 2017 20th International Conference on Electrical Machines and Systems (ICEMS), Sydney, Australia, 11–14 August 2017; pp. 1–6.
3. Khan, F.; Sulaiman, E.; Ahmad, M.Z. A novel wound field flux switching machine with salient pole rotor and nonoverlapping windings. *Turk. J. Electr. Eng. Comput. Sci.* **2017**, *25*, 950–964. [CrossRef]
4. Omar, M.F.; Sulaiman, E.; Jenal, M.; Kumar, R.; Firdaus, R.N. Magnetic Flux Analysis of a New Field-Excitation Flux Switching Motor Using Segmental Rotor. *IEEE Trans. Magn.* **2017**, *53*, 1–4. [CrossRef]
5. Zhu, Z.Q.; Chen, J.T. Advanced flux-switching permanent magnet brushless machines. *IEEE Trans. Magn.* **2010**, *46*, 1447–1453. [CrossRef]
6. Zhao, X.; Niu, S.; Fu, W. Design and comparison of electrically excited double rotor flux switching motor drive systems for automotive applications. *CES Trans. Electr. Mach. Syst.* **2018**, *2*, 191–199. [CrossRef]
7. Taha, M.; Wale, J.; Greenwood, D. Design of a high power-low voltage multiphase permanent magnet flux switching machine for automotive applications. In Proceedings of the 2017 IEEE International Electric Machines and Drives Conference (IEMDC), Miami, FL, USA, 21–24 May 2017; pp. 1–8.
8. Sangdehi, S.; Kazemi, M.; Abdollahi, S.E.; Gholamian, S.A. A segmented rotor hybrid excited flux switching machine for electric vehicle application. In Proceedings of the Power Electronics, Drive Systems & Technologies Conference PEDSTC, Mashhad, Iran, 14–16 February 2017; pp. 347–352.
9. Zhang, G.; Hua, W.; Cheng, M.; Liao, J. Design and comparison of two six-phase hybrid-excited flux-switching machines for EV/HEV applications. *IEEE Trans. Ind. Electron.* **2016**, *63*, 481–493. [CrossRef]
10. Sanabria-Walter, C.; Polinder, H.; Ferreira, J.A.; Jänker, P.; Hofmann, M. Torque enhanced flux-switching PM machine for aerospace applications. In Proceedings of the IEEE International Conference in Electrical Machines ICEM, Marseille, France, 2–5 September 2012; pp. 2585–2595.
11. Chen, Y.; Zhu, Z.Q.; Howe, D. Three-dimensional lumped-parameter magnetic circuit analysis of single-phase flux-switching permanent-magnet motor. *IEEE Trans. Ind. Appl.* **2008**, *44*, 1701–1710. [CrossRef]
12. Tang, Y.; Paulides, J.J.H.; Motoasca, T.E.; Lomonova, E.A. Flux-switching machine with DC excitation. *IEEE Trans. Magn.* **2012**, *48*, 3583–3586. [CrossRef]
13. Rauch, S.E.; Johnson, L.J. Design principles of flux-switch alternators. *Trans. Am. Inst. Electr. Eng. Power Apparatus Syst.* **1955**, *74*, 1261–1268.
14. Pollock, H.; Pollock, C.; Walter, R.T.; Gorti, B.V. Low cost, high power density, flux switching machines and drives for power tools. *Ind. Appl. Conf.* **2003**, *3*, 1451–1457.
15. Pollock, C.; Pollock, H.; Brackley, M. Electronically controlled flux switching motors: A comparison with an induction motor driving an axial fan. *Ind. Electron. Soc. IECON* **2003**, *3*, 2465–2470.
16. Zhou, Y.J.; Zhu, Z.Q. Comparison of low-cost single-phase wound-field switched-flux machines. *IEEE Trans. Ind. Appl.* **2014**, *50*, 3335–3345. [CrossRef]
17. Pang, Y.; Zhu, Z.Q.; Howe, D.; Iwasaki, S.; Deodhar, R.; Pride, A. Investigation of iron loss in flux-switching PM machines. In Proceedings of the 4th IET International Conference on Power Electronics, Machines and Drives (PEMD), York, UK, 2–4 April 2008; pp. 460–464.
18. Zhang, Z.; Tang, X.; Wang, D.; Yang, Y.; Wang, X. Novel Rotor Design for Single-Phase Flux Switching Motor. *IEEE Trans. Energy Convers.* **2018**, *33*, 354–361. [CrossRef]
19. Zulu, A.; Mecrow, B.C.; Armstrong, M. A wound-field three-phase flux-switching synchronous motor with all excitation sources on the stator. *IEEE Trans. Ind. Appl.* **2010**, *46*, 2363–2371. [CrossRef]
20. Zhu, L.; Jiang, S.Z.; Zhu, Z.Q.; Chan, C.C. Analytical methods for minimizing cogging torque in permanent-magnet machines. *IEEE Trans. Magn.* **2009**, *45*, 2023–2031. [CrossRef]
21. Abdollahi, S.E.; Vaez-Zadeh, S. Reducing cogging torque in flux switching motors with segmented rotor. *IEEE Trans. Magn.* **2013**, *49*, 5304–5309. [CrossRef]

22. Hoang, E.; Mohamed, G.; Michel, L.; Bernard, M. Influence of magnetic losses on maximum power limits of synchronous permanent magnet drives in flux-weakening mode. In Proceedings of the Industry Applications Conference, Rome, Italy, 8–12 October 2000; pp. 299–303.
23. Chen, J.T.; Zhu, Z.Q.; Iwasaki, S.; Deodhar, R. Comparison of losses and efficiency in alternate flux-switching permanent magnet machines. In Proceedings of the 2010 XIX International Conference on Electrical Machines (ICEM), Rome, Italy, 6–8 September 2010; pp. 1–6.
24. Calverley, S.D.; Jewell, G.W.; Saunders, R.J. *Saunders. Design of a High Speed Switched Reluctance Machine for Automotive Turbo-Generator Applications*; No. 1999-01-2933; SAE Technical Paper; SAE International: Warrendale, PA, USA, 1999.
25. Thomas, A.S.; Zhu, Z.Q.; Wu, L.J. Novel modular-rotor switched-flux permanent magnet machines. *IEEE Trans. Ind. Appl.* **2012**, *48*, 2249–2258. [CrossRef]